Journal of Materials Research and Technology 36 (2025) 8602–8608

Contents lists available at ScienceDirect

Journal of Materials Research and Technology

journal homepage: www.elsevier.com/locate/jmrt

Benefits of incorporating Dy–Cu alloy via the grain boundary diffusion process in recycled magnets

M.B.S. Dias [a,*], G.Y.S. Shimizu [b], L.L. Azevedo [b], D.L. Rodrigues-Jr [b], W.C. Macedo [c], L.F. Antunes [c], L.U. Lopes [c], P.A.P. Wendhausen [c], R.N. Faria [d], C.A.L. Santos [e], F.A.C. Pastrián [e], F.J.G. Landgraf [b]

[a] SENAI Technology Faculty, Osasco, Brazil
[b] Polytechnic School, University of São Paulo, São Paulo, Brazil
[c] Federal University of Santa Catarina, Florianopolis, Brazil
[d] Institute for Energy and Nuclear Research, São Paulo, Brazil
[e] Institute of Technological Research, University of São Paulo, São Paulo, Brazil

ARTICLE INFO

Handling editor: L Murr

Keywords:
Grain boundary diffusion
Magnetic properties microstructure
Corrosion resistance

ABSTRACT

Nd-Fe-B magnets are a critical material for the green energy transition. However, price volatility makes the supply chain fragile, which makes the recycling process an alternative to reduce dependence on raw materials. Unfortunately, the recycling process introduces oxygen into the magnet, getting worse magnetic properties. Thus, this article studies the effects of the grain boundary diffusion (GBD) process with Dy–Cu slurry on the magnetic and corrosion properties of recycled magnets. As expected, the recycling process reduced the coercivity from 1350 kA/m to 850 kA/m and also decreased the coercivity thermal stability (β) from −0,530 %/°C to of −0.590 %/°C. The introduction of oxygen reduces the amount of the Nd-rich phase, preventing the formation of a grain boundary phase. However, since Nd oxides are more electrochemically stable than the Nd-rich phase, an improvement in corrosion resistance occurred. Regarding the GBD performed at 900 °C increases the coercivity to 1290 kA/m and achieves higher thermal stability (β = −0.54 %/°C) compared to recycled magnets. During GBD, a Dy-rich shell composed of $(Dy + Nd + Pr)_2Fe_{14}B$ was formed around the Φ phase grains. Since Dy locally increases the magnetic anisotropy on the surface of the Φ phase grains, a higher magnetic field is required to nucleate an opposite magnetic domain. Moreover, the recycled magnet treated with GBD at 900 °C exhibits higher corrosion resistance than End-of-Life magnets. In summary, the GBD could be an alternative to partially recover the coercivity of recycled magnets, resulting in a magnet with higher corrosion resistance than End-of-Life magnets.

1. Introduction

Due to their exceptional magnetic properties, Nd-Fe-B magnets are essential for the future of electric and hybrid vehicles, as well as wind power generation [1,2]. Recently, the price of rare-earth permanent magnets has increased significantly, accompanied by new government regulations on the mining, smelting, and trade of rare-earth products [2]. As a result, the energy transition envisioned by clean energy policies could be jeopardized by this supply chain fragility. Thus, recycling end-of-life magnets presents a potential alternative to reduce the demand for raw materials [3–5]. Unfortunately, oxygen uptake during the recycling process can result in a decrease in coercivity [6,7]. The increase in oxygen content during the processing of Nd-Fe-B magnets occurs throughout all stages, but it is particularly critical during phases in which there is an increase in surface area e.g., such as hydrogen decrepitation or fine milling, and in those where the raw material is exposed to high temperatures, such as sintering and heat treatments. This is because, even under a controlled atmosphere (for example, in anaerobic chambers with oxygen levels below 3 ppm), there is always some residual oxygen capable of readily reacting with the raw material [8,9].

It is well known that adding Dy as a substitutional element for Nd in the Φ phase can increase the magnetic anisotropy field of the Φ phase, resulting in higher coercive fields [10]. However, Dy^{3+} ions and Fe form

* Corresponding author.
E-mail address: mateus.dias@sp.senai.br (M.B.S. Dias).

https://doi.org/10.1016/j.jmrt.2025.05.068
Received 15 March 2025; Received in revised form 8 May 2025; Accepted 9 May 2025
Available online 10 May 2025

an antiferromagnetic coupling, which lowers the saturation magnetization and reduces the permanent magnetic remanence [10]. An alternative to address Dy's antagonistic behaviour is the Grain Boundary Diffusion (GBD) process, which involves applying a thin layer of heavy rare-earth alloy to the magnet surface, followed by heat treatment to form a heavy rare-earth shell beneath the surface of the Φ-phase grains. The GBD process has been widely applied to non-recycled Nd-Fe-B magnets, resulting in increased coercivity with minimal impact on remanence [11–17].

It is well known that rare-earth magnets have poor corrosion resistance due to the electrochemical potential created by the contact between the Φ phase ($Nd_2Fe_{14}B$) and the intergranular Nd-rich phase [6, 18–20]. Moreover, these magnets are exposed to harsh conditions during application, such as temperature cycles and the corrosive influence of e-motors, making corrosion resistance a crucial parameter for the effective use of the magnets [21]. An alternative to improve corrosion resistance is adding copper, as its high electrode potential can enhance the stability of the Nd-rich phase. However, if Cu is directly added to the alloy, it could enter the crystal structure of the Φ phase and degrade the magnetic properties of the rare-earth magnet [18]. Thus, the GBD could be an alternative to add Cu, in a controlled manner, only to the Nd-rich phase, improving corrosion resistance without reducing the magnetic properties.

Thus, the present study evaluates the impact of GBD treatment on the magnetic and corrosion properties of recycled magnets. To achieve this, a Dy–Cu slurry was applied to both sides of the recycled magnets, and the samples were subjected to three distinct temperatures (800 °C, 900 °C, and 1000 °C) for 10 h, followed by annealing at 525 °C for 1 h. Thus, the magnetic and corrosion properties of end-of-life, recycled, and recycled + GBD magnets were measured, with the changes in properties explained through microstructure analysis.

2. Methods

2.1. Recycling process

The recycled magnets, measuring 9 mm in diameter and 3 mm in height, were produced using the magnet-to-magnet recycling approach, described as follows: end-of-life magnets, with 15 cm × 10 cm x 8 cm, from out-of-use wind turbines, underwent thermal demagnetization at 550 °C for 1 h under vacuum (~10^{-2} mbar). Afterward, the demagnetized material was ground in a planetary mill until it reached an average particle size of 2 μm and then sieved (32 mesh) to remove any powdered residue that might be highly oxidized, and the larger pieces were sandblasted to remove the outer oxide layer. The end-of-life magnets were then subjected to the hydrogen decrepitation process, promoting the embrittlement of the Φ and grain boundary phases, turning the magnet into a coarse powder.

Subsequently, the magnets were subjected to dehydrogenation under vacuum at 550 °C for 480 min. The coarse powder was ball-milled in a hexane environment to reduce the particle size to approximately 2.35 μm, as measured using an HMK-22 Fisher Sub Sieve Sizer permeameter. The next steps, following traditional powder metallurgy technology, include molding, magnetic alignment (H = 2.5 T), isostatic pressing (60 MPa for 10 s), and finally, sintering at 1100 °C for 1 h. Sintering was followed by two annealing steps: at 800 °C for 1 h and at 525 °C for 1 h under vacuum (~10^{-2} mbar).

2.2. Grain boundary diffusion

To prepare the addition alloy for the GBD, a slurry consisting of hydrogenated $Dy_{70}Cu_{30}$ alloy and isopropyl alcohol in a ratio of 0.4 g/ml was manually applied using a brush to the faces perpendicular to the easy magnetization axis of the recycled magnets. Subsequently, the coated recycled magnets underwent heat treatments at temperatures of 800 °C, 900 °C, and 1000 °C for 10 h, followed by annealing at 525 °C for 1 h. Each of these treatments was performed under vacuum (~10^{-4} mbar) with heating and cooling rates of 5 °C/min. A brief description of the experimental conditions for the samples can be found in Table 1.

2.3. Chemical and magnetic characterizations

The chemical composition of the magnets under end-of-life, recycled, and GBD (900 °C) conditions was determined using the ICP-OES technique (ONH836 Elemental Analyzer, LECO), and can be found in Table 2. The compositions for GBD at 800 °C and 1000 °C are very similar to that at 900 °C and are therefore not presented.

Regarding the oxygen level, the values for end-of-life and recycled magnets were 1520 ± 150 ppm and 2700 ± 315 ppm, respectively. The values for remanence, coercivity, squareness factor, and temperature coefficients were determined from demagnetization curves obtained using the Hystograph (HG 200, Brockhauss Messtechnik GmbH & Co.).

2.4. Microstructural characterization

Initially, the magnets were metallographically prepared using sandpaper grades #500, #1200, and #2000, and polished with diamond paste of 6 μm, 3 μm, 1 μm, and 0.25 μm. Subsequently, the prepared samples were analysed using a Field Emission Gun Scanning Microscope, model Inspect F-50 (Thermo). Moreover, to identify the presence of a Dy-rich shell on the grain boundaries, energy dispersive X-ray spectroscopy (EDS) was performed using an Edax sensor attached to the FEG-SEM microscope.

2.5. Corrosion resistance characterization

The electrochemical impedance spectroscopy (EIS) measurements were performed with a PAR-Versastat 3–400 over a frequency range of 50 kHz to 0.01 Hz, using a sinusoidal signal perturbation amplitude of 0.01 V. Ten points per decade were acquired. A three-electrode cell arrangement was employed with the following configuration: working electrode (studied sample); reference electrode (Ag/AgCl 0.1 mol/L KCl); auxiliary electrode (high-purity graphite bar). A 0.10 mol/L NaCl naturally aerated solution, maintaining a neutral pH (6.8–7.2), was used as the electrolyte.

Before the EIS measurements, the studied samples were kept under open circuit potential (OCP) recording for 7200 s (2 h). The EIS results were fitted by Zview® software.

3. Results

3.1. Magnetic characterizations

The demagnetization curves of the End-of-Life, recycled magnets, and GBD magnets are compared in Fig. 1.

Following the recycling process, the remanence remains unchanged, while coercivity values decrease from approximately 1500 kA/m to around 850 kA/m; however, the squareness factor (SF) values for the End-of-Life and recycled magnets remain high, achieving 0.95 and 0.9, respectively.

For all three temperatures applied in GBD, it is possible to observe that the remanence remains barely the same for all recycled and GBD magnets, which was already expected since the amount of Dy added by Dy–Cu slurry is small [11]. Moreover, a reduction in SF occurred after the GBD, achieving values of 0.61, 0.77, and 0.60 for the treatments performed at 800 °C, 900 °C, and 1000 °C, respectively. Regarding the GBD performed at 800 °C and 1000 °C, the coercivity values decrease from 810 kA/m (recycled magnet) to 650 kA/m and 740 kA/m, respectively, as shown in Fig. 1(b) and (c). However, an improvement in coercive field was achieved for the GBD magnets subjected to 900 °C, where the coercivity increased to 1290 kA/m. The magnetic properties of all sample conditions can be found in Table 1.

Table 1
Description of experimental condition and magnetic properties of all studied samples.

Samples condition	High temperature annealing?	Low temperature annealing (800 °C and 525 °C)?	Addition of Dy–Cu slurry?	Br (T)	Hc (kA/m)	SF (ratio)
End-of-life	No	No	No	1.2	−1350	0.95
Recycled	No	Yes	No	1.2	−850	0.90
GBD (800 °C)	Yes (800 °C)	Yes	Yes	1.2	−650	0.61
GBD (900 °C)	Yes (900 °C)	Yes	Yes	1.2	−1290	0.77
GBD (1000 °C)	Yes (1000 °C)	Yes	Yes	1.2	−740	0.60

Table 2
Chemical composition by ICP-OES of end-of-life magnets, recycled magnets, and recycled magnets followed by the GBD process.

Chemical Element	Cu	Fe	Dy	Nd	Pr	(rare-earth sum)[a]
End-of-life magnet	0.37 %	69.2 %	0.73 %	24.53 %	4.35 %	**30,41 %**
Recycled magnet	0.28 %	70.28 %	0.78 %	23.63 %	4.17 %	**29,42 %**
GBD (900 °C) magnet	0.47 %	69.46 %	1.55 %	23.54 %	4.14 %	**30,05 %**

[a] Corresponds to the sum of Dy + Pr + Nd.

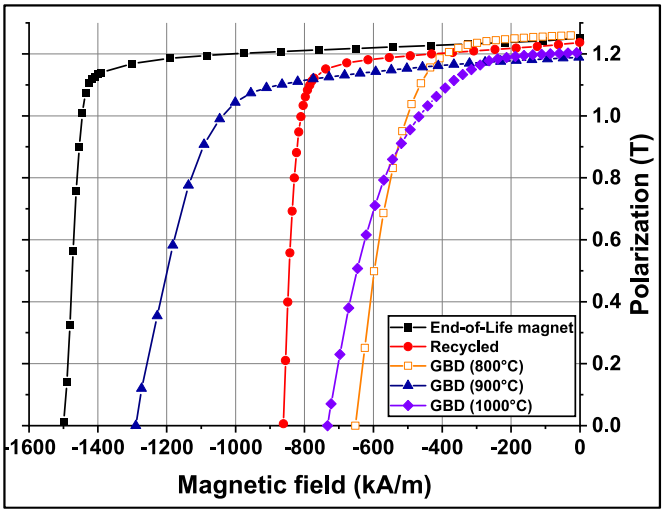

Fig. 1. Demagnetization curves for the End-of-Life (black square), recycled magnets (red circle), and GBD (800 °C) (yellow open square), GBD (900 °C) (blues triangle), and GBD (1000 °C) (purple diamond).

The variations in remanence and coercivity for the End-of-Life, recycled, and optimal GBD treatment (i.e., at 900 °C) are shown in Fig. 2(a) and (b).

For all three conditions, there is a decrease in both remanence and coercivity values as the temperature increases. This decrease in remanence is attributed to the loss of magnetization as the temperature rises, particularly when the temperature approaches the Curie temperature (Tc) [22]. Similarly, the decrease in coercivity can be attributed to the increase in thermal energy and the reduction of the anisotropy field (Ha), which facilitates changes in the orientation of the magnetic moment, thereby reducing the magnet's resistance to external magnetic fields [23].

Regardless of the condition, the temperature coefficient of remanence (α) did not show a significant change, achieving −0.140 ± 0.005 %/°C, −0.150 ± 0.006 %/°C, and −0.150 ± 0.002 %/°C for the End-of-Life, Recycled, and GBD (900 °C) magnets, respectively. However, the temperature coefficient of coercivity (β) decreased after the recycling process, reducing from −0.53 ± 0.008 %/°C to −0.59 ± 0.002 %/°C. After the GBD treatment, β decreased to −0.54 ± 0.005 %/°C, indicating that this condition is more thermally stable compared to the recycled one [24].

3.2. Microstructure characterization

A microstructure obtained using the BSE-SEM mode and chemical composition measured by energy dispersive spectroscopy (EDS) of the End-of-Life, recycled, recycled magnets subjected to the GBD process at 800 °C, 900 °C, and 1000 °C can be seen in Fig. 3, and Table 3, respectively. The EDS points shown in Table 2 are identified by the numbers presented in Fig. 3, and additional EDS results can be found in Supplementary material A.

As expected from the literature [15,25], the BSE-SEM and EDS analyses confirm the presence of the Φ phase $(Nd + Pr)_2Fe_{14}B$ (dark grey), Nd-rich phase (bright regions), Nd oxides (grey regions in high relief), and the grain boundary phase in the End-of-Life magnet (cf. Fig. 3 (a)).

Although the same phases were identified after the recycling process, three main microstructural changes occurred: a reduction in the Nd-rich

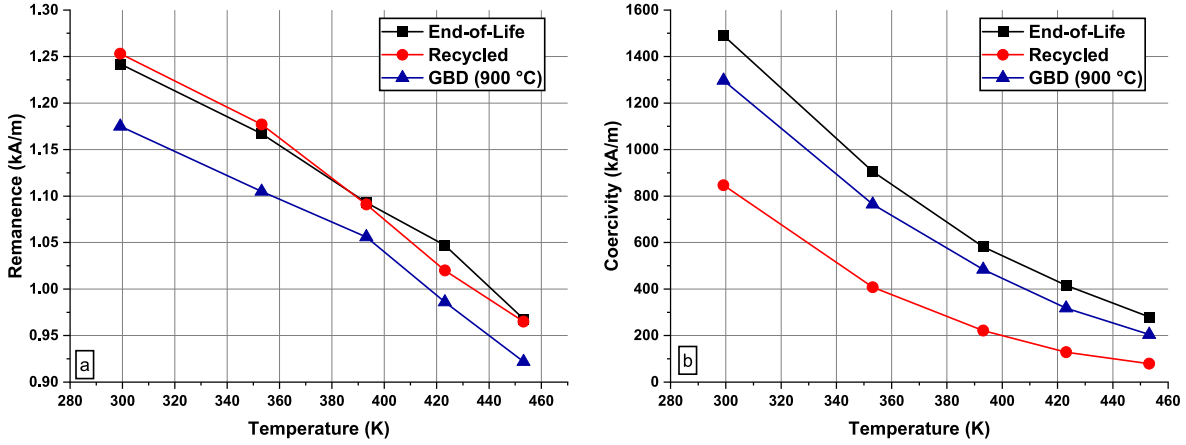

Fig. 2. Temperature dependency of remanence and coercivity for the End-of-Life (black curve), recycled (red curve) and recycled + GBD (900 °C) (blue curve) magnets.

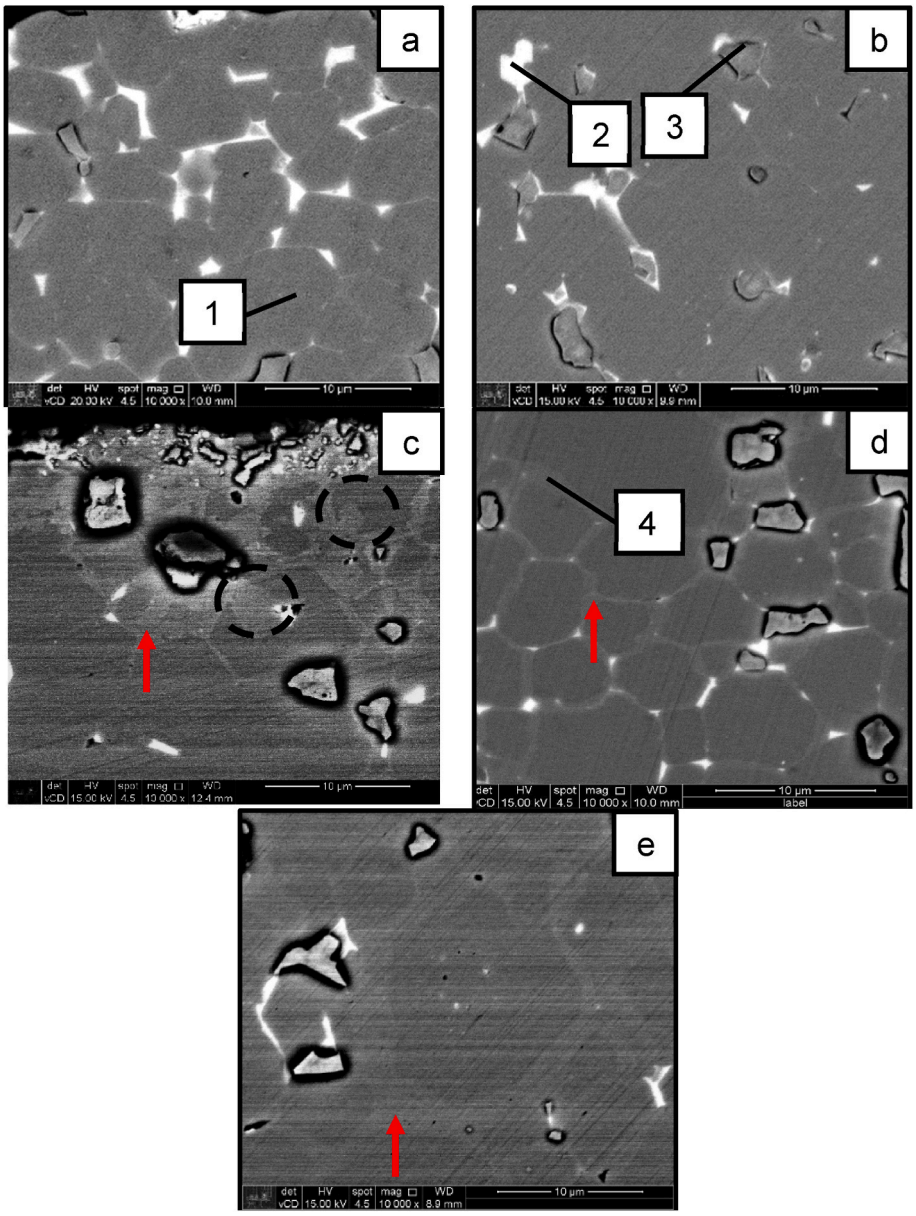

Fig. 3. BSE-SEM image of End-of-Life (a), recycled magnet (b), GBD magnets treated at 800 °C (c), GBD magnets treated at 900 °C (d), and GBD magnets treated at 1000 °C (e).

Table 3
Chemical composition measured by EDS.

Points	Chemical Element (at.%)					
	Fe	O	Dy	Pr	Nd	(rare-earth sum)[a]
1 (cf. Fig. 3) - Φ phase	86.5	0	0	3	10.5	13.5
2 (cf. Fig. 3) - Nd-rich phase	41.9	0	0	19.3	38.8	58.1
3 (cf. Fig. 3) -(Nd + Pr)$_x$O$_y$	6.6	55.4	0	9.4	28.8	38.2
4 (cf. Fig. 3) - Dy-rich shell	86.6	0	4.6	1.8	7.1	13.5

[a] Corresponds to the sum of Dy + Pr + Nd.

phase volume fraction, an increase in the Nd_yO_x volume fraction, and a reduction in the grain boundary phase thickness.

First, the volume fraction of the Nd-rich phase reduced from 9.8 % ± 2.0 % (end-of-life magnet) to 4.5 % ± 1.8 % after the magnet was recycled. The measurement procedure and the values used to calculate the mean values are presented in Supplementary material B.

Secondly, the oxygen content, measured by ICP-OES, in the recycled magnets reached 2700 ± 315 ppm, which is higher than the 1520 ± 150 ppm found in the End-of-Life magnet. Consequently, the volume fraction of the Nd_yO_x oxides increased from 3.9 ± 0.9 % in the End-of-Life magnet to 7.4 ± 1.6 % in the recycled magnet. Last but not least, as shown in Fig. 3 (b), the grain boundary phase is less pronounced in the recycled magnet, indicating a reduction in its thickness [25].

Regardless of the temperature used in the GBD treatment, a new light grey region can be observed around the Φ-phase, as indicated by the red arrows in Fig. 3(c–e). Since the contrast in SEM images varies with chemical composition, it is expected that this region contains heavier elements than the inner area of the Φ-phase grain. Therefore, an EDS map was acquired for a magnet subjected to GBD at 800 °C (see Fig. 4) to identify the chemical composition of this new region. The EDS maps obtained at other temperatures are very similar and are not shown.

Based on the EDS maps, it is evident that partial substitution of Nd by

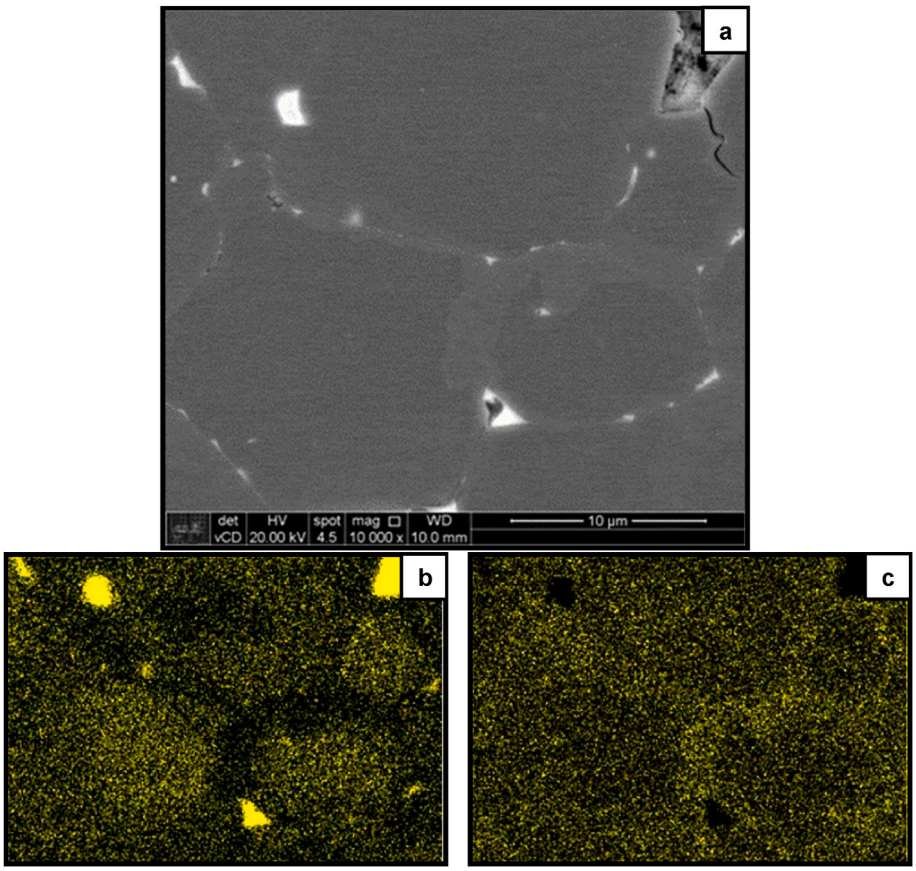

Fig. 4. Microstructure of recycled magnet subjected to GBD at 800 °C, showing the (a) original image, (b) EDS maps for Nd, and (c) EDS maps for Dy.

Dy occurred after the GBD treatment, which explains the lighter contrast observed in this region. Furthermore, point analysis using EDS (see Table 2) shows that inside the Φ-phase (Point 1 of Table 3), the rare-earth elements present are only Nd (10.5 at.%) and Pr (3.0 at.%), resulting in a total rare-earth content (Nd + Pr) of 13.5 at.%. Point 4 in Table 3 represents the Dy-rich shell, where the composition includes Nd (7.1 at.%), Pr (1.8 at.%), and Dy (4.6 at.%), confirming the EDS map results shown in Fig. 4. It is important to emphasize that the total rare-earth content (Nd + Pr + Dy) in the Dy-rich shell remains the same as in the inner region of the grains, with a total of 13.5 at.%. A comparison of the rare-earth content across different magnet phases is presented in Table 3. The formation of a Dy-rich shell around the Φ-phase grains after GBD treatment has been previously reported in the literature [2,11–14,26].

For all GBD temperature treatments, the depth of Dy diffusion, where a Dy-rich shell can be identified beneath the Φ-phase grains, is significantly less than the total thickness of the magnet, indicating that Dy is concentrated only near the surface. For the GBD treatments performed at 800 °C, 900 °C, and 1000 °C, the average Dy diffusion depths were 18.3 ± 7.1 μm, 65.8 ± 7.8 μm, and 89.2 ± 5 μm, respectively. More information on how the average Dy diffusion depth was measured can be found in Supplementary material C. The concentration of the heavy rare-earth element close to the surface was already reported for non-recycled magnets [24,27,28].

These distinct values of Dy diffusion depths for different GBD temperatures have already been reported for non-recycled magnets [11]. However, the depths found in the recycled samples are smaller than those in non-recycled magnets from Ref. [11], which could indicate that the higher amount of Nd_yO_x may hinder Dy diffusion during the GBD process. A similar result was observed in the case of GBD performed with Tb [24].

Moreover, the magnets subjected to GBD at 800 °C and 1000 °C show worse magnetic properties than the recycled ones, indicating that the GBD treatment must be optimized to produce magnets with higher coercive fields. In the case of the magnets treated at 800 °C, beyond the low Dy diffusion depth (18 ± 6.8 μm), the Dy-rich shell is irregular, where it is possible to easily find regions of the shell entering inside the grain (cf. dotted lines in Fig. 3 (c)). With reference to the GBD performed at 1000 °C, grain growth also occurred, resulting in a reduction of the coercive field. Therefore, an antagonistic effect occurs at this temperature, in which the beneficial effect of Dy-rich shell is balanced by grain growth, producing worse magnetic properties for the recycled magnet, as can be seen in Fig. 1 (c). It is important to emphasize that grain growth has already been reported in non-recycled magnets subjected to GBD at 1000 °C for 6 h [11].

3.3. Corrosion resistance

The OCP curves show a decrease in potential values for all three conditions studied, as shown in Fig. 5.

The decrease in potential values for all studied conditions is attributed to the dissolution of the oxide films formed during the surface preparation of the samples; subsequently, the potential values increase and stabilize, reaching a steady state condition. After 7200 s, the open circuit potential value for the End-of-Life sample (−0.84 V) is approximately 20 mV lower than those observed for the GBD (900 °C) (−0.82 V) and Recycled (−0.81 V) samples. Since the potential value indicates corrosion susceptibility, the End-of-Life magnets have the worst corrosion resistance, followed by the GBD (900 °C), with the Recycled magnets showing the best corrosion resistance.

As shown in Fig. 5, all samples exhibit similar Nyquist plot shapes, indicating that the same corrosion mechanism is observed [20]. The flattened semicircles, observed at frequencies ranging from 50 kHz to 0.5 Hz, correspond to the active dissolution of the samples due to

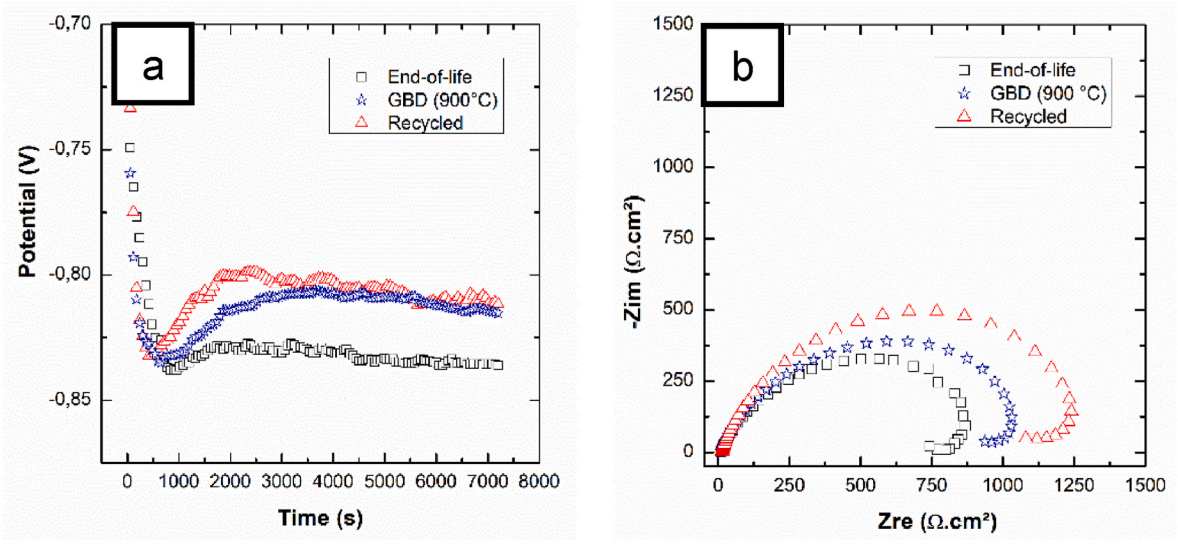

Fig. 5. Open circuit potential curves (a) and Nyquist plots (b) from Nd-Fe-B samples: End-of-Life (black square), GBD (900 °C) (blue star) and Recycled (red triangle).

corrosion processes [20]. The inductive loops at low frequencies (10 mHz) can be attributed to adsorption processes [29], such as the adsorption of corrosion products formed during open circuit potential monitoring or the breakdown of the oxide films through pit corrosion of the sample's substrate [30]. The charge transfer resistance (Rct_0) values for the Nd-Fe-B substrate samples are 857.7 Ω cm^2 (End-of-life), 963.1 Ω cm^2 (GBD at 900 °C), and 1118.0 Ω cm^2 (Recycled). These values demonstrate that the GBD process at 900 °C provides better corrosion resistance compared to the End-of-life magnet samples, probably due to the copper diffusion into the rich phase [15,24].

4. Discussion

4.1. Effects of recycling

After the recycling process, a significant increase in oxygen content was observed in the recycled magnets [6], rising from 1520 ± 150 ppm to 2700 ± 315 ppm. This oxygen reacts with the Nd-rich phase to form hexagonal close-packed (Nd_2O_3) and/or face-centered cubic (NdO) oxides at triple junctions [6,31], thereby reducing the volume fraction of the Nd-rich phase. Since the Nd-rich phase melts during post-sintering annealing to form the grain boundary phase [14,31–33], its transformation into oxides after the recycling process may reduce the amount of liquid formed during low-temperature annealing [31,34]. This reduction could decrease the grain boundary phase thickness, consequently increasing the magnetic coupling between the Φ-phase grains. Thus, this magnetic coupling is responsible for the decrease in coercivity and the higher value of |β| observed after the recycling process. On the other hand, the Nd oxides are more stable than the Nd-rich phase; consequently, the recycled magnets exhibit greater corrosion resistance compared to the End-of-Life magnets.

4.2. Effects of GBD

The addition of Dy–Cu slurry during the GBD facilitated the formation of a $(Nd + Pr + Dy)_2Fe_{14}B$ shell (Dy-rich shell) on the surface of the grains, thereby increasing the local magnetic anisotropy [10,12,24]. Consequently, the reverse magnetic domain nucleation requires a higher magnetic field, as evidenced by the increased coercive field observed in the GBD (900 °C) samples. Furthermore, β also depends on Ha; therefore, the incorporation of heavy rare-earth, e.g., Dy, into the Φ-phase grains enhances the thermal stability of Nd-Fe-B magnets, explaining the reduction of β to −0.54 %/°C [10,15,24,35].

However, no increase in coercive field was observed for the magnets subjected to GBD at 800 °C and 1000 °C. Thus, factors beyond Dy-rich shell formation must be considered when evaluating the temperature efficiency of the GBD treatment. In the case of GBD performed at 900 °C, the Dy-rich shell is more uniform compared to the magnets subjected to GBD at 800 °C and does not promote grain growth as observed with GBD performed at 1000 °C.

It is well known that coercivity is inversely proportional to grain size [2]; therefore, the GBD will only be effective if the Dy-rich shell does not promote grain growth. A similar behaviour of the effects of GBD temperatures on magnetic properties was already observed in Ref. [11] for a non-recycled magnet.

For all the temperatures used in the GBD, the Dy-rich shell was only observed close to the magnet surface, with diffusion depths of 18 ± 6.8 μm, 66.6 ± 7.9 μm, and 89.1 ± 4.7 μm for the temperatures of 800 °C, 900 °C, and 1000 °C, respectively. Thus, since the entire magnet's thickness is 3000 μm, the heterogeneous magnetic properties across the magnet thickness explain the reduction in the squareness factor (SF) after the GBD, going from 0.9 (recycled magnet) to 0.61, 0.77, and 0.60 for the GBD performed at 800 °C, 900 °C, and 1000 °C, respectively [36].

When compared to the recycled magnet, a reduction in corrosion resistance occurs after the GBD at 900 °C due to the addition of the Dy element. However, since a considerable amount of the Nd-rich phase still partially oxidizes after this treatment and Cu was added during the GBD with Dy–Cu, its corrosion resistance is higher than that of the End-of-Life magnet.

5. Conclusions

This work evaluates the beneficial effects of GBD on the magnetic and corrosion properties of recycled magnets.

The undesirable introduction of oxygen during the recycling process is the main factor responsible for the considerable reduction in coercive field and thermal stability. This element reacts with the Nd-rich phase, forming oxides; as a result, the small amount of liquid phase during low-temperature annealing prevents the formation of the grain boundary diffusion phase, promoting magnetic coupling between the Φ phase grains.

An alternative to partially recovering the coercivity of recycled magnets is the GBD performed at 900 °C, where a uniform Dy-rich shell form around the Φ phase grains. This shell increases both coercivity and thermal stability due to the presence of Dy, which enhances the magnetic anisotropy. However, the GBD performed at 800 °C and 1000 °C

did not increase the coercivity, as the Dy-rich shell was not uniformly formed in these conditions, and grain growth occurred, which counteracts the desired effect on magnetic properties. For all the studied temperatures, the formation of the Dy-rich shell occurred only near the surface of the magnet, which contributed to the reduction in the squareness factor of the hysteresis loops.

Finally, the oxidation of the Nd-rich phase during the recycling process enhances the corrosion resistance, making the GBD treatment at 900 °C exhibit better corrosive properties than the End-of-Life magnet.

In summary, the GBD performed at 900 °C could serve as an alternative to improve the coercivity of recycled magnets without reducing corrosion resistance.

Declaration of competing interest

The authors declare that they have no known competing financial interests or personal relationships that could have appeared to influence the work reported in this paper.

Acknowledgements

This study was financed by the São Paulo Research Foundation (FAPESP) Brazil, [Process Number #2014/50887-4, #2023/06160-1, #2023/06403-1], Conselho Nacional de Desenvolvimento Científico e Tecnologico (CNPq) [grant number #308991/2022-2, and INCT-PATRIA Project through grant number 88882.345177/2014-01 and #465719/2014-7], and by the Financier of Studies and Projects (FINEP) through grant number 01.23.0478.00 (2457/22).

Appendix A. Supplementary data

Supplementary data to this article can be found online at https://doi.org/10.1016/j.jmrt.2025.05.068.

References

[1] Rizos V, Righetti E, Kassab A. Developing a supply chain for recycled rare earth permanent magnets in the EU. CEPS - EU, https://www.ceps.eu/ceps-publications/developing-a-supply-chain-for-recycled-rare-earth-permanent-magnets-in-the-eu/. [Accessed 23 December 2023].
[2] Nakamura H. The current and future status of rare earth permanent magnets. Scr Mater 2018;154:273–6. https://doi.org/10.1016/j.scriptamat.2017.11.010.
[3] U.S. DEPARTMENT OF ENERGY. Critical materials strategy. 2011.
[4] Ormerod J, Karati A, Baghel APS, Prodius D, Nlebedim IC. Sourcing, refining and recycling of rare-earth magnets. Sustainability 2023;15:14901. https://doi.org/10.3390/su152014901.
[5] Heim JW, Vander Wal RL. NdFeB permanent magnet uses, projected growth rates and Nd plus Dy demands across end-use sectors through 2050: a review. Minerals 2023;13:1274. https://doi.org/10.3390/min13101274.
[6] Pan M, Liu X, Jin W, Fu S, Yang E, Liu X, et al. Effect of Cu grain boundary modification on microstructure and corrosion resistance in recycled Nd-Fe-B sintered magnets. J Magn Magn Mater 2022;550:169109. https://doi.org/10.1016/j.jmmm.2022.169109.
[7] Edgley DS, Le Breton JM, Steyaert S, Ahmed FM, Harris IR, Teillet J. Characterisation of high temperature oxidation of NdFeB magnets. J Magn Magn Mater 1997;173:29–42. https://doi.org/10.1016/S0304-8853(97)00189-3.
[8] Li WF, Ohkubo T, Hono K, Sagawa M. The origin of coercivity decrease in fine grained Nd–Fe–B sintered magnets. J Magn Magn Mater 2009;321:1100–5. https://doi.org/10.1016/j.jmmm.2008.10.032.
[9] Sepehri-Amin H, Une Y, Ohkubo T, Hono K, Sagawa M. Microstructure of fine-grained Nd–Fe–B sintered magnets with high coercivity. Scr Mater 2011;65:396–9. https://doi.org/10.1016/j.scriptamat.2011.05.006.
[10] Sagawa M, Hirosawa S, Tokuhara K, Yamamoto H, Fujimura S, Tsubokawa Y, et al. Dependence of coercivity on the anisotropy field in the $Nd_2Fe_{14}B$-type sintered magnets. J Appl Phys 1987;61:3559–3561. https://doi.org/10.1063/1.338725.
[11] Löewe K, Brombacher C, Katter M, Gutfleisch O. Temperature-dependent Dy diffusion processes in Nd–Fe–B permanent magnets. Acta Mater 2015;83:248–55. https://doi.org/10.1016/j.actamat.2014.09.039.
[12] Hirota K, Nakamura H, Minowa T, Honshima M. Coercivity enhancement by the grain boundary diffusion process to Nd–Fe–B sintered magnets. IEEE Trans Magn 2006;42:2909–11. https://doi.org/10.1109/TMAG.2006.879906.
[13] Hu S, Peng K, Chen H. Influence of annealing temperature on the Dy diffusion process in NdFeB magnets. J Magn Magn Mater 2017;426:340–6. https://doi.org/10.1016/j.jmmm.2016.11.111.
[14] Sepehri-Amin H, Ohkubo T, Hono K. The mechanism of coercivity enhancement by the grain boundary diffusion process of Nd–Fe–B sintered magnets. Acta Mater 2013;61:1982–90. https://doi.org/10.1016/j.actamat.2012.12.018.
[15] Huang YL, Rao Q, Feng Q, Wu ZJ, Yao YF, Hou YH, et al. An insight into the improved microstructure and elevated comprehensive properties of sintered Nd-Fe-B magnets via the infiltration of DyCu alloy. J Mater Res Technol 2022;20:3094–102. https://doi.org/10.1016/j.jmrt.2022.08.088.
[16] Li W, Zhang Q, Zhu Q, Xiao S, Xu C, Yang L, et al. Formation of anti-shell/core structure of heavy rare earth elements (Tb, Dy) in sintered Nd-Fe-B magnet after grain boundary diffusion process. Scr Mater 2019;163:40–3. https://doi.org/10.1016/j.scriptamat.2018.12.034.
[17] Ji M, Liu W, Wang Z, Wu H, Du R, Li Y, et al. The reinforcement strategy of electrophoretic deposition coating assisted by PVP for grain boundary diffusion of Nd-Fe-B magnet. J Mater Res Technol 2024;28:3068–75. https://doi.org/10.1016/j.jmrt.2023.12.237.
[18] Zhang P, Ma T, Liang L, Yan M. Improvement of corrosion resistance of Cu and Nb co-added Nd–Fe–B sintered magnets. Mater Chem Phys 2014;147:982–6. https://doi.org/10.1016/j.matchemphys.2014.06.046.
[19] El-Moneim AA, Gebert A, Schneider F, Gutfleisch O, Schultz L. Grain growth effects on the corrosion behavior of nanocrystalline NdFeB magnets. Corros Sci 2002;44:1097–112. https://doi.org/10.1016/S0010-938X(01)00123-8.
[20] Shao Y, Ni J, Wang Z, Wang X, Xu K, Song B, et al. Relations of magnetic and electrochemical anti-corrosion properties of (Zr, Ti)-doped NdCeFeB magnets with Ti content. J Mater Res Technol 2024;33:4083–91. https://doi.org/10.1016/j.jmrt.2024.10.120.
[21] Moore M, Sueptitz R, Gebert A, Schultz L, Gutfleisch O. Impact of magnetization state on the corrosion of sintered Nd-Fe-B magnets for e-motor applications: Nd-Fe-B magnets in e-motor applications. Mater Corros 2014;65:891–6. https://doi.org/10.1002/maco.201206978.
[22] Herbst JF. R 2 Fe 14 B materials: intrinsic properties and technological aspects. Rev Mod Phys 1991;63:819–98. https://doi.org/10.1103/RevModPhys.63.819.
[23] Vial F, Joly F, Nevalainen E, Sagawa M, Hiraga K, Park KT. Improvement of coercivity of sintered NdFeB permanent magnets by heat treatment. J Magn Magn Mater 2002;242–245:1329–34. https://doi.org/10.1016/S0304-8853(01)00967-2.
[24] Mo Z, Jiang Q, Kan M, Li J, Wang H. Comparison of microstructures and magnetic properties of Tb-Pr-Cu-Al and Tb-Nd-Cu-Al grain boundary diffused Nd-Fe-B magnets. J Mater Res Technol 2025;35:1865–74. https://doi.org/10.1016/j.jmrt.2025.01.137.
[25] Li WF, Ohkubo T, Akiya T, Kato H, Hono K. The role of Cu addition in the coercivity enhancement of sintered Nd-Fe-B permanent magnets. J Mater Res 2009;24:413–20. https://doi.org/10.1557/JMR.2009.0041.
[26] Qin Y, Li Y, Wang Z, Wu H, Zhang L, Liu W, et al. Analysis on coercivity enhancement mechanism of grain-boundary-diffused and Dual-alloyed Nd-Fe-B Magnets. J Mater Res Technol 2024;29:1805–12. https://doi.org/10.1016/j.jmrt.2024.01.245.
[27] Zhou T, Liu R, Qu P, Xie G, Li M, Zhong Z. Diffusion behavior and coercivity enhancement of Tb-containing NdFeB magnet by dip-coating TbH3. J Mater Res Technol 2022;20:1391–8. https://doi.org/10.1016/j.jmrt.2022.07.167.
[28] Zhan H, Peng C, Xue Y, Wang X, Lin X, Bai X, et al. Effect of different deposition sequences on the magnetic properties of sintered Nd–Fe–B magnets diffused with multicomponent Tb–Cu films. J Mater Res Technol 2023;27:3161–9. https://doi.org/10.1016/j.jmrt.2023.10.181.
[29] Dai J, Yang Z, Liu Q. Rare earth cerium increases the corrosion resistance of NdFeB magnets. Materials 2020;13:4360. https://doi.org/10.3390/ma13194360.
[30] Wu Y, Zhu M, Shen P, Fang Y, Sun Q, Zhang L, et al. A design of sintered Nd-Fe-B magnet exhibiting superior corrosion resistance based on the metallurgical behavior of Ni and Cr. J Mater Res Technol 2023;24:6369–77. https://doi.org/10.1016/j.jmrt.2023.04.218.
[31] Sasaki TT, Ohkubo T, Hono K. Structure and chemical compositions of the grain boundary phase in Nd-Fe-B sintered magnets. Acta Mater 2016;115:269–77. https://doi.org/10.1016/j.actamat.2016.05.035.
[32] Sepehri-Amin H, Ohkubo T, Shima T, Hono K. Grain boundary and interface chemistry of an Nd–Fe–B-based sintered magnet. Acta Mater 2012;60:819–30. https://doi.org/10.1016/j.actamat.2011.10.043.
[33] Li WF, Ohkubo T, Hono K. Effect of post-sinter annealing on the coercivity and microstructure of Nd–Fe–B permanent magnets. Acta Mater 2009;57:1337–46. https://doi.org/10.1016/j.actamat.2008.11.019.
[34] Shinba Y, Konno TJ, Ishikawa K, Hiraga K, Sagawa M. Transmission electron microscopy study on Nd-rich phase and grain boundary structure of Nd–Fe–B sintered magnets. J Appl Phys 2005;97:053504. https://doi.org/10.1063/1.1851017.
[35] Cui J, Ormerod J, Parker D, Ott R, Palasyuk A, Mccall S, et al. Manufacturing processes for permanent magnets: Part I—sintering and casting. J Occup Med 2022;74:1279–95. https://doi.org/10.1007/s11837-022-05156-9.
[36] Wang Z, Yue M, Liu W, Li Y, Wu H, Liu Y, et al. Tuning the distribution of Tb in Nd-Fe-B sintered magnet to overcome the magnetic properties trade-off. Scr Mater 2022;217:114789. https://doi.org/10.1016/j.scriptamat.2022.114789.